Refractive index dispersion of chalcogenide glasses for ultra-high numerical-aperture fiber for mid-infrared supercontinuum generation

Dantanarayana, Harshana G.; Abdel-Moneim, Nabil; Tang, Zhuoqi; Sojka, Lukasz; Sujecki, Slawomir; Furniss, David; Seddon, Angela B.; Kubat, Irnis; Bang, Ole; Benson, Trevor M.

Published in:
Optics Express

Link to article, DOI:
10.1364/OME.4.001444

Publication date:
2014

Document Version
Publisher's PDF, also known as Version of record

Refractive index dispersion of chalcogenide glasses for ultra-high numerical-aperture fiber for mid-infrared supercontinuum generation

Harshana G. Dantanarayana,[1] Nabil Abdel-Moneim,[1,2] Zhuoqi Tang,[1,2] Lukasz Sojka,[1,2] Slawomir Sujecki,[1] David Furniss,[1,2] Angela B. Seddon,[1,2] Irnis Kubat,[3] Ole Bang,[3] and Trevor M. Benson[1,*]

[1]*George Green Institute for Electromagnetics Research Faculty of Engineering, University of Nottingham, University Park, Nottingham, NG7 2RD, UK*

[2]*Mid-Infrared Photonics GroupFaculty of Engineering, University of Nottingham, University Park, Nottingham, NG7 2RD, UK*

[3]*DTU Fotonik, Dept. of Photonics Engineering, Technical University of Denmark, Ørsteds Plads 343, 2800 Kongens Lyngby, Denmark*

**Trevor.Benson@nottingham.ac.uk*

Abstract: We select a chalcogenide core glass, AsSe, and cladding glass, GeAsSe, for their disparate refractive indices yet sufficient thermal-compatibility for fabricating step index fiber (SIF) for mid-infrared supercontinuum generation (MIR-SCG). The refractive index dispersion of both bulk glasses is measured over the 0.4 μm–33 μm wavelength-range, probing the electronic and vibrational behavior of these glasses. We verify that a two-term Sellmeier model is unique and sufficient to describe the refractive index dispersion over the wavelength range for which the experimentally determined extinction coefficient is insignificant. A SIF composed of the glasses is fabricated and calculated to exhibit an ultra-high numerical aperture >0.97 over the entire wavelength range 0.4-33 μm suggesting that the SIF glass pair is a promising candidate for MIR-SCG. Material dispersion characteristics and the zero dispersion wavelength, both critical design parameters for SIF for MIR-SCG, are derived.

OCIS codes: (160.2750) Glass and other amorphous materials; (060.2310) Fiber optics; (320.6629) Supercontinuum generation.

References and Links

1. A. B. Seddon, "Chalcogenide glasses: a review of their preparation, properties and applications," J. Non-Cryst. Solids **184**, 44–50 (1995).
2. J. M. Harbold, F. O. Ilday, F. W. Wise, J. S. Sanghera, V. Q. Nguyen, L. B. Shaw, and I. D. Aggarwal, "Highly nonlinear As-S-Se glasses for all-optical switching," Opt. Lett. **27**(2), 119–121 (2002).
3. A. B. Seddon, "A prospective for new mid-infrared medical endoscopy using chalcogenide glasses," Int. J. Appl. Glass Sci. **2**(3), 177–191 (2011).
4. A. B. Seddon, "Mid-infrared (IR) – a hot topic, the potential for using mid-IR light for non-invasive, early detection of skin cancers in vivo," Phys. Status Solidi B **250**(5), 1020–1027 (2013).
5. Z. G. Lian, Q. Q. Li, D. Furniss, T. M. Benson, and A. B. Seddon, "Solid microstructured chalcogenide glass optical fibers for the near-and mid-infrared spectral regions," IEEE Photon. Technol. Lett. **21**(24), 1804–1806 (2009).
6. Y. Yu, X. Gai, T. Wang, P. Ma, R. Wang, Z. Yang, D.-Y. Choi, S. Madden, and B. Luther-Davies, "Mid-infrared supercontinuum in chalcogenides," Opt. Mater. Express **3**(8), 1075–1086 (2013).
7. W. Yuan, "2–10μm mid-infrared supercontinuum generation in As2Se3 photonic crystal fiber," Laser Phys. Lett. **10**(9), 095107 (2013).
8. I. Kubat, C. R. Petersen, U. V. Møller, A. Seddon, T. Benson, L. Brilland, D. Méchin, P. M. Moselund, and O. Bang, "Thulium pumped mid-infrared 0.9-9μm supercontinuum generation in concatenated fluoride and chalcogenide glass fibers," Opt. Express **22**(4), 3959–3967 (2014).
9. C. Agger, C. Pedersen, S. Dupont, H. Steffensen, J. K. Lyngsø, C. L. Thomsen, J. Thøgersen, S. R. Keiding, and O. Bang, "Supercontinuum generation in ZBLAN fibers – detailed comparison between measurement and simulation," J. Opt. Soc. Am. B **29**(4), 635–645 (2012).
10. Amorphous Materials Inc, "AMTIR-2 Information" (consulted July 2013). http://www.amorphousmaterials.com/app/download/6552914504/Amtir-2+Information.pdf.

#210165 - $15.00 USD Received 14 Apr 2014; revised 4 Jun 2014; accepted 13 Jun 2014; published 27 Jun 2014

11. D. Furniss and A. B. Seddon, "Thermal analysis of inorganic compound glasses and glass-ceramics" in *Principles and Applications of Thermal Analysis*, Paul Gabbott, ed. (Wiley-Blackwell, 2007), Chap. 10.
12. G. Jellison and F. Modine, "Parameterization of the optical functions of amorphous materials in the interbandregion," Appl. Phys. Lett. **69**(3), 371–373 (1996).
13. G. E. Jellison, "Data analysis for spectroscopic ellipsometry," in *Handbook of Ellipsometry*, H. G. Tompkins and E. A. Irene, ed. (William Andrew, Inc., 2005), Chap. 3.
14. A. S. Ferlauto, G. M. Ferreira, J. M. Pearce, C. R. Wronski, R. W. Collins, X. Deng, and G. Ganguly, "Analytical model for the optical functions of amorphous semiconductors from the near-infrared to ultraviolet: Applications in thin film photovoltaics," J. Appl. Phys. **92**(5), 2424–2436 (2002).
15. A. Zakery and S. R. Elliott, *Optical Nonlinearities in Chalcogenide Glasses and their Applications* (Springer, 2007).
16. M. S. Maklad, R. K. Mohr, R. E. Howard, P. B. Macedo, and C. T. Moynihan, "Multiphonon absorption in As2S3-As2Se3 glasses," Solid State Commun. **15**(5), 855–858 (1974).
17. E. Palik, *Handbook of optical constants of solids*, vol. 3, (Academic Press, 1998).
18. J. Orava, J. Šik, T. Wagner, and M. Frumar, "Optical properties of $As_{33}S_{67-x}Se_x$ bulk glasses studied by spectroscopic ellipsometry," J. Appl. Phys. **103**(8), 083512 (2008).
19. H. Dantanarayana, "Application of TLM for optical microresonators," Ph.D. thesis, Faculty of Engineering, The University of Nottingham,UK, (2012).
20. H. Dantanarayana, A. Vukovic, P. Sewell, Z. Lian, D. Furniss, A. Seddon, E. Romanova, A. Konyukhov, B. Derkowska, J. Orava, T. Wãgner, and T. Benson, "The optical properties of chalcogenide glasses: From measurement to electromagnetic simulation tools," in *Proceedings of 12th International Conference on Transparent Optical Networks (ICTON)* (2010), pp. 1–4.
21. G. P. Agrawal, *Nonlinear Fiber Optics* (5th edition, Academic Press, 2013).
22. I. Shavrin, S. Novotny, and H. Ludvigsen, "Mode excitation and supercontinuum generation in a few-mode suspended-core fiber," Opt. Express **21**(26), 32141–32150 (2013).
23. J. M. Dudley, G. Genty, and S. Coen, "Supercontinuum generation in photonic crystal fiber," Rev. Mod. Phys. **78**(4), 1135–1184 (2006).
24. B. Ung and M. Skorobogatiy, "Chalcogenide microporous fibers for linear and nonlinear applications in the mid-infrared," Opt. Express **18**(8), 8647–8659 (2010).

1. Introduction

The chalcogenide glasses [1] are based on Group 16 elements of the Periodic Table: S, Se and Te, usually formulated with additions of Group 14 and Group 15, such as the germanium and arsenic elements, respectively, to increase glass stability and robustness. The chalcogenide glasses are amorphous semiconductors, exhibiting an optical band-gap. They combine low phonon energy and high optical nonlinearity [2]; hence chalcogenide-glass optical fibers are suitable as mid-infrared (MIR, 3-25 microns) supercontinuum generation (SCG) sources. The advent of bright, broadband MIR-SCG fiber sources will enable developments in the new field of remote, real-time molecular sensing and spectral imaging with a huge impact across many sectors, including: mid-IR medical endoscopic systems for real-time sensing, imaging and analysis of tissue [3,4] (*thereby hastening diagnosis, medical decisions and treatment-planning*); remote monitoring of manufacturing and chemical processes (*thereby enabling process-control and product quality control*); remote, real-time sensing of explosives and narcotics *for security purposes*; sensing of exhaust gases for *real-time monitoring of environmental-quality and energy-efficiency* and also sensing in food production and security.

In this work, we have selected two chalcogenide glass compositions: AsSe ($As_{40}Se_{60}$ atomic% (at%)) and GeAsSe ($Ge_{10}As_{23.4}Se_{66.6}$ at%) [5] as the core and cladding glasses, for a step-index fiber (SIF) for MIR-SCG. The AsSe core and GeAsSe cladding glass pair was chosen to give not only ultra-disparate refractive indices for ultra-high numerical aperture (*NA*) SIF, but also to have sufficient thermal-compatibility above and below the glass transition (T_g) in order to enable fiber fabrication [5]. The purpose of the high-NA chalcogenide fiber is to allow guidance over the whole transparency region, which includes most of the so-called molecular fingerprint region. In particular, the high NA and high nonlinearity would allow supercontinuum generation to potentially span the low loss region.

Material dispersion data are required to guide the design of chalcogenide glass SIF for MIR-SCG [6–8] that go beyond the transparency region of about 5 μm of other MIR SIF, such as ZBLAN [9]. However, few dispersion data are available in the MIR and far-infrared (FIR, 25-50 μm wavelength range) for the chalcogenide glasses [10]. Here, we have measured refractive index dispersion of the AsSe core and GeAsSe cladding glasses from the visible

#210165 - $15.00 USD Received 14 Apr 2014; revised 4 Jun 2014; accepted 13 Jun 2014; published 27 Jun 2014

region (VIS: 0.4-0.7 μm), through the near-infrared (NIR: 0.7-3 μm), MIR (3-25 μm) and into the FIR (limited here up to 33 μm by the ellipsometer employed). We verify that a two-term type Sellmeier model is unique and sufficient to describe the refractive index dispersion of each glass. Material dispersion of the glasses and the zero dispersion wavelengths are derived and the variation of numerical aperture (*NA*) with wavelength is calculated for SIF, comprised of the AsSe core and GeAsSe cladding glasses.

2. Preparation of glass samples for the refractive index dispersion measurement

2.1. Glass melting

Arsenic (7N, Furukawa Electric Ltd.) and selenium (5N, Cerac) were pre-purified by heating under vacuum (10^{-3}Pa) at 310°C and 270°C, respectively; Ge (5N, Cerac) was used as-received. The AsSe core and the GeAsSe cladding glass precursors were each batched into a pre-purified, silica-glass-ampoule which was then evacuated and sealed. Glass melting was carried out with rocking at 800°C / 12h. The melt was cooled *in situ* to 650°C, air-quenched and then held immersed vertically for 1 minute in a furnace, which had been pre-heated to the onset-T_g. Quenching was completed under N_2 gas-jet cooling as the ampoule was gradually withdrawn from the furnace. The rod-shaped glass product was then annealed by heating at the onset-T_g for 2 h, followed by cooling with the furnace. Onset-T_g is defined here as the extrapolated onset [11] of the T_g event in the differential scanning calorimetry (DSC) run carried out at a heating rate of 10°C/min and immediately after a controlled pre-treatment of the glass sample comprising heating at 10°C/min to above the T_g event on the DSC curve then cooling at 10°C/min to ambient in the calorimeter before the actual run. It is important to specify the thermal history of the glasses in this way as refractive index varies with the glass fictive temperature [11].

2.2. Sample preparation

A glass disc of 10 mm diameter and 1.7 mm thick was cut (Leco, diamond wafer blade) from each of the AsSe and GeAsSe annealed glass rods. Disc faces were ground (SiC, Buehler, 1000 grit) and successively polished to a 1 μm finish. To ensure that the opposite faces of the discs were both flat, orthogonal to the rod axis and parallel, the disc samples were lightly hot-pressed under vacuum at T_g + 25°C, between two tungsten carbide discs (each ≈ 100 mm diameter, of flatness 0.08 μm and of surface finish 0.009 μm). The samples were then annealed at the onset-T_g and allowed to cool with the press. After the hot-pressing, the back face of each disc was re-roughened (SiC, Buehler, 1000 grit), while the polished, pressed front disc-face was protected with Parafilm M©. The final AsSe and GeAsSe disc thicknesses were 1.04 mm and 1.06 mm, respectively.

3. Refractive index dispersion measurements

The AsSe core and GeAsSe cladding bulk glass samples (prepared as in section 2.2), were analyzed by means of spectroscopic ellipsometry at ambient temperature (298K) at incident angles 55° to 75°, in 10° intervals; the incident angle range was close to the Brewster angle, in order to collect the data in the angular region with most sensitivity to the reflection differences between p- and s- polarized light. Over the 140 nm–1700 nm wavelength-range the Woollam UVU VASE rotating analyzer ellipsometer was used to measure refractive index and the entire optical path was enclosed inside a dry nitrogen purge to eliminate absorption from ambient water vapor and oxygen. Over the 1.7 μm – 33 μm wavelength-range, the refractive index was measured by means of the Woollam IR-VASE rotating compensator ellipsometer.

Ellipsometry uses polarized light to characterize materials; the change in light polarization is measured after reflecting the light from the material-surface and, if the material is isotropic and ideal, then this may be expressed as two parameters: ψ (related to phase) and Δ (related to amplitude), for each wavelength/angle combination. The incident-angle dependence of ψ, and of Δ, is defined by the complex ratio of the p- and s- polarized Fresnel reflection coefficients: r_p and r_s, respectively, as given in Eq. (1) [12].

#210165 - $15.00 USD Received 14 Apr 2014; revised 4 Jun 2014; accepted 13 Jun 2014; published 27 Jun 2014

$$\frac{r_p}{r_s} = tan\,\psi \times exp(j\,\Delta) \tag{1}$$

WVASE32 version 3.774 was used to analyze the raw data. The standard practice of data analysis followed in order to eliminate noise is to assume a refractive index model or a combination of models (as in the present case) and the presence of an effective medium to represent surface roughness [13]. The unknown properties of the sample are defined as model fit parameters which the software adjusts recursively to obtain agreement between modeled and measured data. In the present work a Cody-Lorentz function along with multiple Gaussian oscillators was used to model the absorption spectrum of the AsSe core glass and GeAsSe cladding glass samples. The Cody-Lorentz function models the imaginary part of the permittivity (ε_2) as shown in Eq. (2) [14]:

$$\varepsilon_2(E) = \begin{cases} \dfrac{E_1}{E} exp\left(\dfrac{E - E_t}{E_u}\right); & 0 < E \le E_t \\ \dfrac{\left(E - E_g\right)^2}{\left(E - E_g\right)^2 + E_p^2} \dfrac{AE_0\Gamma E}{\left[\left(E^2 - E_0^2\right)^2 + \Gamma^2 E^2\right]}; & E > E_t \end{cases} \tag{2}$$

where: E is the photon energy in eV and E_0, E_1, E_u, E_g, E_t, E_p, A and Γ are fitting parameters in eV [14]. E_t is identified as the demarcation energy between the Urbach tail transitions and band-to-band transitions [14].

Using the Kramers-Kronig relations shown in Eq. (3), a wavelength-dependent real part of the permittivity function (ε_1) was obtained [12]:

$$\varepsilon_1(E) = \varepsilon_1(\infty) + \frac{2}{\pi} \wp \int_0^\infty \frac{\xi \varepsilon_2(\xi)}{\xi^2 - E^2}\, d\xi \tag{3}$$

where $\varepsilon_1(\infty)$ is a constant and $\wp$ denotes the Cauchy principal value of the integral and ξ is the energy dummy variable.

A Sellmeier dispersion function was superimposed on this real part of the permittivity model to obtain a complete model of the complex permittivity for each glass composition. Hence, using the relationships: $\varepsilon_1 = n^2 - \kappa^2$ and $\varepsilon_2 = 2n\kappa$, the refractive index (n) and the extinction coefficient (κ) were calculated. The model fitted a surface roughness layer on each glass sample, composed equally of glass and void (air) in an effective medium approximation, of 5.5 nm depth for the AsSe sample and of 2.3 nm depth for the GeAsSe sample. The depth of this layer was a parameter determined in the regression analysis to best-fit the models. The root-mean-square angular error between the measured ψ and Δ values and the modeled values was ≈ 0.5° for both samples.

Figure 1 shows the refractive index (n) dispersion curves and the variation of the extinction coefficient (κ) with wavelength, which were calculated from the ellipsometry measurements of the AsSe core and GeAsSe cladding bulk glass samples.

From Fig. 1, the steeply rising extinction coefficient with decreasing wavelength starting from ~650 nm (GeAsSe), and ~700 nm (AsSe), which reaches a maximum extinction coefficient at ~ 1.7, is proposed to be associated with the optical band-gap electronic absorption of each of the two glasses.

Zakery and Elliott [15] describe the optical band-gap of amorphous semiconductors as divisible into three parts:

- for α (absorption coefficient) > 10^4 cm^{-1}, a square root dependence is found with frequency

#210165 - $15.00 USD Received 14 Apr 2014; revised 4 Jun 2014; accepted 13 Jun 2014; published 27 Jun 2014

• for 10^4 cm^{-1} ≥ α ≥ 10^0 cm^{-1}, the dependence is exponential ('Urbach' edge)

• for α < 10^0 cm^{-1}, the dependence is also exponential ('Weak Absorption Tail')

Plotting $(\alpha h\upsilon)^{1/2}$ *versus* hυ (where υ is photon frequency and h is Planck's constant) above the Urbach edge yields a straight line and it is generally accepted that the optical band-gap of the amorphous chalcogenides may be defined as the intersection of this straight line with the energy axis. Applying this method, Zakery and Elliott [15] reported the optical band-gap as 701 nm, and 645 nm, for $As_{40}Se_{60}$ (at%) and $Ge_9As_{25}Se_{66}$, respectively, which are coincident with the onset of rising extinction coefficient with decreasing wavelength of ~ 700 nm for the $As_{40}Se_{60}$ and ~ 650 nm for the $Ge_{10}As_{23.4}Se_{66.6}$ glass found here (Fig. 1).

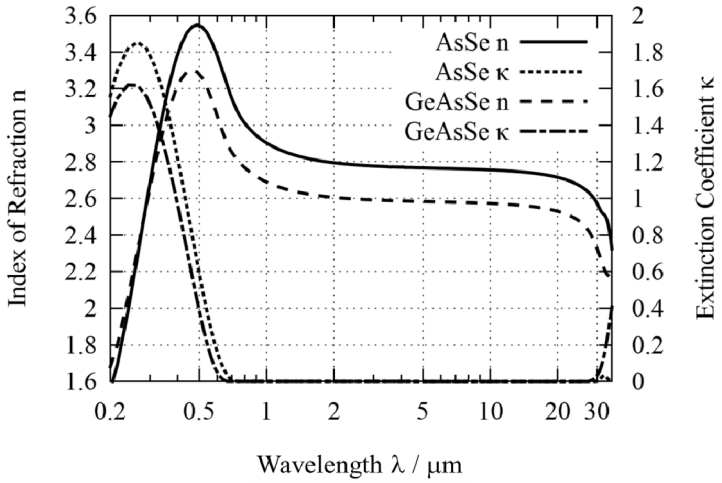

Fig. 1. Refractive index (*n*) and extinction coefficient (*κ*) variation with wavelength calculated from the ellipsometry measurements of the AsSe core and GeAsSe cladding bulk glass samples.

Also in Fig. 1, the onset rise in extinction coefficient with wavelength at ~ 30 microns wavelength is noticeable for the AsSe and GeAsSe glass samples and is due to fundamental vibrational absorption [16].

4. Refractive index models

4.1 Glass transparent window

From the ellipsometry measurements here, despite the refractive index/wavelength data being calculated to five significant digits from the raw ellipsometric measurements, the modeled refractive index and extinction coefficient were prudently only taken as accurate up to four significant digits. As a consequence, the transparent region of each glass sample was taken to be where the extinction coefficient (*κ*) was smaller than 0.0005, which was the region extending from ~ 0.7 μm to ~ 30 μm wavelength, according to the extinction coefficient plot in Fig. 1. An extinction coefficient of 0.0005 corresponds to a loss of 390 dB/cm at a wavelength of 0.7 μm, and 9 dB/cm at a wavelength of 30 μm. The group of Moynihan [16] has applied infrared spectroscopy of $As_{40}Se_{60}$, of very short optical path-length samples - down to 18 μm, to study the spectral region of intrinsic overtone and combination bands occurring from 7.7 μm to 33 μm wavelength. According to Moynihan and his co-workers [16], the optical loss of $As_{40}Se_{60}$ in this wavelength region exhibits a maximal absorption coefficient (α) of 35 cm^{-1} at 20.8 μm (a combination band) and at ~ 33 μm (rising absorbance and the limit of their study) wavelengths. This would correspond to a loss of 152 dB/cm at both wavelengths. This loss value is greater than the limit of transparency as defined above (where the extinction coefficient (*κ*) is smaller than 0.0005); so this absorption should have been apparent on the extinction coefficient *vs.* wavelength plot here (Fig. 1), and indeed was

#210165 - $15.00 USD Received 14 Apr 2014; revised 4 Jun 2014; accepted 13 Jun 2014; published 27 Jun 2014

at 33 μm wavelength, but not at 20.8 μm wavelength. It is worth noting that this combination band at 20.8 μm wavelength was identified in the study of Moynihan's group's [16] as $2\upsilon_s$, the second overtone of the fundamental stretching band (υ_s) due to $AsSe_3$ pyramid units in the $As_{40}Se_{60}$ glass structural matrix. Therefore the fundamental stretching band (υ_s) was calculated [16] to occur at 41.7 μm wavelength, but was not observable using the technique of Moynihan and his co-workers [16]. The second maximal loss occurred almost coincident with a shoulder (on a rising loss curve) assigned to the fundamental stretching (υ_b) of bent As-Se-As bridges in the $As_{40}Se_{60}$ glass structural matrix and calculated to occur at 29.4 μm wavelength [16].

For realizing MIR-SCG SIF, the fiber optical loss should be minimized to < 0.1 dB/cm: which is only achievable, for the AsSe and GeAsSe glasses studied, in a limited wavelength window between the optical band-gap intrinsic absorption and a point in the overtone and combination band MIR spectral region; we term this window, of loss < 0.1 dB/cm, the *useable* glass transparent window and it is appropriate for applications like passively transmitting MIR-SIF and for active SIF for MIR-SCG. Of course, in reality the *useable* glass transparent window will be compromised by extrinsic scattering loss and extrinsic absorption loss in the glasses and loss due to waveguide geometrical imperfections.

4.2 Refractive index models

Once the complex refractive index of a particular sample has been measured at several wavelengths, a model is required which will interpolate the data points and represent the characteristic in as few coefficients as possible. Two such models, which are well known [17], are the Sellmeier model, given in Eq. (4), and the Cauchy model, given in Eq. (5):

$$n^2 - 1 = A_0 + \sum_{n=1}^{N} \frac{A_n \lambda^2}{\lambda^2 - a_n^{\,2}} \tag{4}$$

$$n^2 - 1 = A + \frac{B}{\lambda^2} + \frac{C}{\lambda^4} \tag{5}$$

where: A_0 and A_n are dimensionless coefficients; a_n are the material resonant wavelengths; N denotes the number of resonance terms; λ is wavelength and A, B, C are Cauchy fitting coefficients.

For the chalcogenide glasses and other semiconductor materials [12], a Tauc-Lorentz model has also previously been employed to represent the complex refractive index in the VIS-to-NIR spectral regions [18], around the optical band-gap. Due to the piecewise nature of the Tauc-Lorentz model, its general implementation in time-domain-type numerical modeling has proved impractical [19]. On the other hand, both the Sellmeier and Cauchy models are not only simple in concept but also material dispersion may be obtained from the second derivatives of Eq. (4) and Eq. (5). The Cauchy model in this form does not encompass the entire glass transparent window (defined in 4.1) and so the Sellmeier model was rather applied here.

The Sellmeier model embodies a number of resonances in the material. Due to the theoretically unbounded nature of the material resonances (*i.e.* the right hand side of Eq. (5) becomes infinite as $\lambda \rightarrow a_n$), the Sellmeier model can only be applied to the non-absorbing spectral region of the material, defined here as the transparent window region (section 4.1). The Sellmeier model is non-analytical and this precluded determination of the corresponding imaginary part of the refractive index related to loss. The Tauc-Lorentz model on the other hand expresses the complex refractive index *via* the Kramers-Kronig relationship [12] but is only applicable around the optical bandgap absorption spectral region. For the MIR-SCG applications considered here, the dispersion characteristics in the transparent window of the glass and, even more pertinently, the *useable* window (see section 4.1) are more important than accurate modeling of the imaginary part of the complex refractive index (permittivity) of the optical band-gap edge, which have been shown to reach a loss in excess of ~ 10^6 dB/cm

#210165 - $15.00 USD Received 14 Apr 2014; revised 4 Jun 2014; accepted 13 Jun 2014; published 27 Jun 2014

[15]. Moreover, the Sellmeier model has been shown to provide accuracy for As-(Ge)-Se glass compositions in representing the real part of the refractive index in the useable window, for which the extinction coefficient was more negligible [19,20].

4.3 Fitting procedure

Unlike the Cauchy model, which is a simple polynomial, when fitting to a Sellmeier model using a linear least square fitting (LSF) algorithm, more attention to detail is required for setting the initial parameters. Since the Sellmeier model becomes unbounded at resonance frequencies, the a_n parameters must be initially placed outside the transparent window fitting region, *i.e* placed here at wavelengths for which the extinction coefficient was > 0.0005 (section 4.1).

In [20], As-(Ge)-Se chalcogenide glasses were modeled accurately only up to 2.3 μm wavelength in the NIR using one Sellmeier term in the VIS region and a constant. Moreover, the wavelength range of the refractive index measurement data available did not enable the authors of [20] to model the material zero dispersion wavelength, which would have required experimental data for wavelengths extending beyond the NIR, into the MIR and FIR. In contrast, our refractive index measurements here encompassed the complete glass transparency window (see section 4.1) and beyond, spanning the 0.4 μm–33 μm wavelength-range, to model the chalcogenide glasses.

Depending on the choice of a_n parameters, several different sets of Sellmeier coefficients can be obtained. However, not all of these models tend to a physical interpretation and this would be an advantage in giving insight not only into the dispersion characteristic but also into the electronic and vibrational characteristics of the material. In addition, it is convenient to have a unique set of Sellmeier coefficients independent of the fitting procedure (*i.e.* independent of the initial parameters, reduced mean squared error *etc.*).

From Fig. 1, due to the discontinuity of the Sellmeier model at a_1, and a_2, these were allowed to vary below 0.7 μm, and above 33μm, respectively, in the fitting process. Accordingly, this has been named the Sellmeier II (1,1) model to signify two resonances: one in the VIS-NIR and one in the FIR region. Coefficients A_0, A_1 were initialized at 1 and were allowed to take any real value. At the end of the fitting procedure, the fitted parameter co-variances were smaller than 0.1%, indicating that the coefficients were convergent for the model sought.

In order to test whether we could achieve a lower modeling error by introducing a third Sellmeier term, two Sellmeier III models were fitted with the extra term: a_3 , and A_3, in the VIS-NIR (named: Sellmeier III (2,1)) and FIR regions (named: Sellmeier III (1,2)), respectively. When a_3 was placed in the VIS-NIR part of the spectrum, it was given an initial value of 0.7 μm and was allowed to vary below 0.7 μm. When a_3 was placed in the FIR region, it was given an initial value of 33 μm and was allowed to vary above 33 μm. A_3 was initialised at 1 and was allowed to take any real value. The refractive index fitting error percentages for the three models for As-Se, and Ge-As-Se glasses, are shown in Fig. 2(a) and(b), respectively. The final Sellmeier coefficients used for the three types of fittings are provided in Table 1 for reference.

4.4 Sellmeier model parameters

From Fig. 2(a) and Fig. 2(b), all three models provide a good fit to the refractive index dispersion accurate up to 0.1%, within the transparent window (section 4.1). Moreover, the Sellmeier II model (two terms: a_1 and a_2) was found to be a sufficient and unique model to represent accurately the two As-(Ge)-Se chalcogenide glasses across their transparent window. Closer examination of Table 1 shows that the effect of the extra Sellmeier term a_3 , was simply to split one of the existing resonances into two resonances, close together, without increasing the fitting accuracy significantly.

For the Sellmeier II model (two terms: a_1 and a_2), the physical significance of a_1 and a_2 for the AsSe glass is now considered. a_2 is associated with vibrational band resonant absorption. The value of a_2 from the Sellmeier II model is 41.395 μm which fits well with the position of

#210165 - $15.00 USD Received 14 Apr 2014; revised 4 Jun 2014; accepted 13 Jun 2014; published 27 Jun 2014

the fundamental stretching band (υ_s) calculated to occur at 41.7 μm and due to stretching of $AsSe_3$ pyramid units in the $As_{40}Se_{60}$ glass structural matrix [16]. This suggests that the refractive index dispersion might be predicted from knowledge of the fundamental resonant absorptions of a chalcogenide glass. Turning to the Sellmeier II model for the GeAsSe glass, a_2 is a vibrational resonance at 38.537 μm, at shorter wavelength than a_2 of the AsSe glass (41.395 μm).

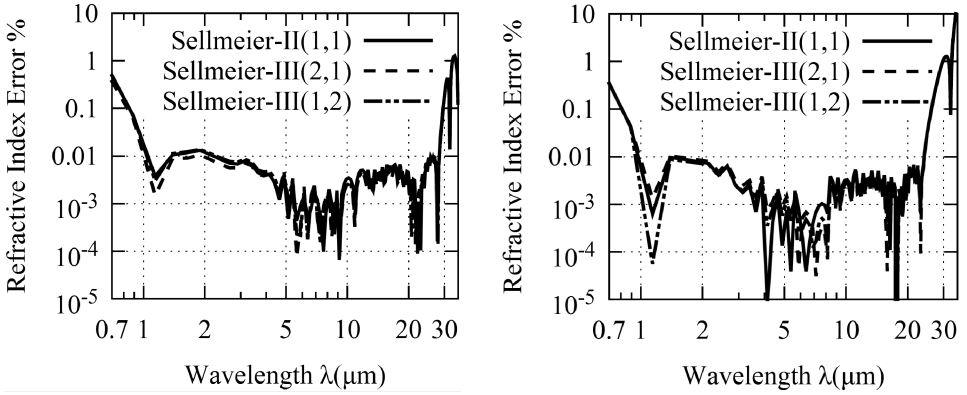

Fig. 2. Refractive index modeling error of < 0.1% for: (a) AsSe and (b) GeAsSe, using models: Sellmeier II (1VIS, 1FIR), Sellmeier III (2 VIS,1 FIR) and Sellmeier III (1 VIS,2 FIR).

For AsSe, a less good fit to known resonant absorption is found for the Sellmeier II a_1 coefficient than for the Sellmeier II a_2 coefficient. The Sellmeier II a_1 coefficient is associated with the optical bandgap absorption. As mentioned earlier (section 3 [15],), the optical bandgap of $As_{40}Se_{60}$ has been calculated to be at 701 nm which is quite different from the a_1 value for the AsSe glass here of 438 nm. The extinction coefficient, calculated from the refractive index data measured here, at 701 nm [15] is low enough to lie within the as-defined transparent window (section 4.1). For the moment, this precludes the Sellmeier II model for these chalcogenide glasses being wholly predictable from known absorption coefficient data.

Nevertheless, we have presented the unique and complete dispersion relationship in the whole transparency window, for the AsSe and the GeAsSe chalcogenide glass compositions. The advantage of having a unique set of coefficients is that from a literature of glass chemical composition/molecular structure and unique Sellmeier II coefficients, one might correlate the dispersion and glass chemical composition or even molecular structure. With refinement, this could eventually allow one to reverse engineer glasses to produce a suitable glass composition for a particular application requiring certain dispersion characteristics.

We compare now the AsSe Sellmeier II model coefficients (two terms: a_1 and a_2) with those published for AMTIR-2: an AsSe glass of similar, but not identical, composition to that used in the current work (AMTIR-2: reported T_g is 10K-15K lower, implying an enriched Se content compared to $As_{40}Se_{60}$) described in the literature [10]. The AMTIR-2 Sellmeier model coefficients published in [10] are not coincident with absorption bands, especially the longer quoted [10] resonance at 19 μm. We suggest that this is at least in part due to the fact that refractive index data in only a limited region (1 μm to 13 μm) were available to those authors. Hence, the resonant wavelength of the long wavelength Sellmeier term would essentially have become a free parameter, and in [10], was fixed at 19 μm. According to the Moynihan *et al.* [15] study, the closest absorption band to 19 μm is the second overtone of the fundamental absorption at 41.7 μm occurring at 20.8 μm); it is concluded that the choice of fixing the Sellmeier parameter at 19 μm was not rigorous [10].

#210165 - $15.00 USD Received 14 Apr 2014; revised 4 Jun 2014; accepted 13 Jun 2014; published 27 Jun 2014

Table 1. Sellmeier coefficients of As-Se and Ge-As-Se glasses. The numbers in parentheses correspond to the number of material resonances in the VIS and the FIR, respectively. AMTIR-2 data for As-Se, rearranged to see correspondence, is from reference [10].

	Sellmeier II (1,1)	Sellmeier III(2,1)	Sellmeier III(1,2)	AMTIR II [4]
			As-Se	
A_0	3.3344	2.5611	3.3337	
A_1	3.3105	1.9098	3.3111	1.308575
a_1	0.43834 μm	0.47350 μm	0.43830 μm	$2a_3$=0.48328 μm
A_2	0.89672	0.89565	1.1850	0.347441
a_2	41.395 μm	41.383 μm	41.226 μm	19 μm
A_3		2.1738	-0.28860	2.234921
a_3		0.31202 μm	40.742 μm	0.24164 μm
			Ge-As-Se	
A_0	2.7742	1.2966	2.7741	
A_1	2.8928	2.7616	2.8928	
a_1	0.40470 μm	0.40801 μm	0.40470 μm	
A_2	0.73204	0.73204	0.84788	
a_2	38.537 μm	38.524 μm	38.291 μm	
A_3		1.6087	-0.11740	
a_3		0.095693 μm	37.060 μm	

4.5 SIF and numerical aperture

SIF multimode fiber based on the AsSe core and GeAsSe cladding glasses has been successfully fabricated. Figure 3(a) is a scanning electron micrograph (SEM) of the cross-section of sample of the cleaved multimode SIF. Figure 3(b) shows the SEM energy dispersive X-ray analysis (EDX) Ge elemental mapping of the fiber cross-section. Ge was found only in the surrounding cladding (GeAsSe) and not in the core (AsSe), as expected. Further details about this fiber, and small core fiber, will form the basis of another publication, but we note here that the *useable* glass transparency window of this fiber, based on our criterion of loss <0.1dB/cm, is from 0.7-11.7 μm.

The numerical aperture (*NA*) of the SIF composed of the designed glass pair was calculated from:

$$NA = \sqrt{n_1^2 - n_2^2} \tag{6}$$

where n_1 and n_2 are the refractive indices of the core AsSe glass, and the cladding GeAsSe glass, respectively, comprising the optical fiber. As shown in Fig. 4, SIFs constructed from this AsSe/GeAsSe glass pair had a calculated *NA* greater than 0.97 over the entire wavelength range of refractive index measurement by means of ellipsometry: 0.4-33 μm. This ultra-high *NA* allows the core modes to be strongly confined in the fiber core (*i.e.* strong guiding) and theoretically a MIR-SC to be unhindered across the wavelength range, making this glass pair a promising candidate for SIF MIR-SCG. The large NA will naturally make the fiber multi-moded, as is well-known in step-index optical fiber theory; see for example [21]. However, only very few of these modes will be guided above 5μm and through good coupling the number of excited modes can be significantly reduced. Using short pump pulses to increase intermodal temporal walk-off modal issues can be further reduced, as demonstrated by, e.g., Shavrin *et al.* [22].

#210165 - $15.00 USD Received 14 Apr 2014; revised 4 Jun 2014; accepted 13 Jun 2014; published 27 Jun 2014

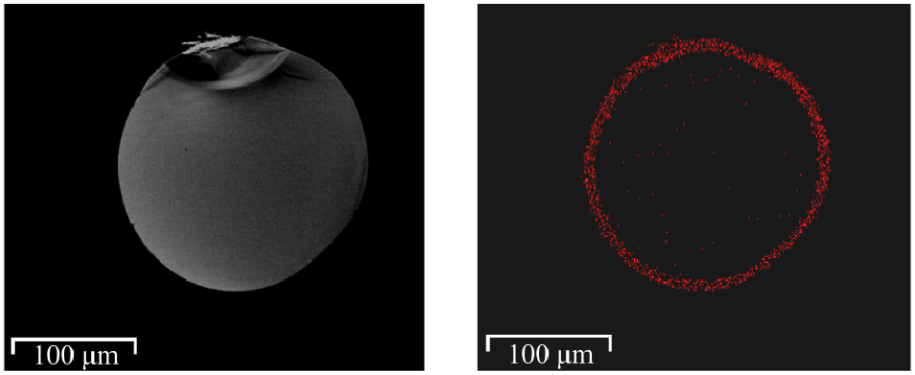

Fig. 3. SIF multimode fiber comprising an AsSe glass core and GeAsSe glass cladding: (a) scanning electron micrograph (SEM) of the cross-sectional view of the multimode fiber and (b) SEM energy dispersive X-ray analysis (EDX) Ge elemental mapping of the fiber cross-section where Ge was found only in the surrounding cladding (GeAsSe) and not in the core (AsSe), as expected.

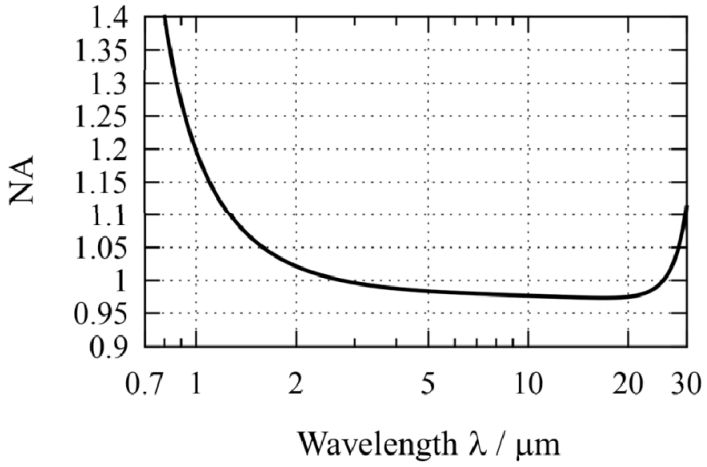

Fig. 4. *NA* variation with wavelength for an optical fibre comprised of the AsSe glass core and GeAsSe glass cladding.

4.6 Dispersion

Supercontinuum generation in simple step-index optical fibers depends critically on both optical confinement and the dispersion tailoring [23]. Efficient SCG may require pumping in the anomalous dispersion regime, close to the material zero-dispersion wavelength (ZDW) [23]. Pumping in the anomalous dispersion region close to the material ZDW with high power lasers causes the long wavelength edge of the SC eventually to be determined by a number of solitons red-shifting due to the Raman effect. For femtosecond pumping, the solitons will be generated by soliton fission; for long-pulse pumping (picosecond to CW (continuous wave)) the solitons will be generated when the pump breaks up due to modulation instability. To exist, the solitons require anomalous dispersion and to red-shift efficiently the dispersion should be weak. Therefore, for the spectral broadening to continue to long wavelengths, the dispersion should remain anomalous and weak in a correspondingly broad wavelength-region. Hence, it is critical to know the dispersion characteristics not just around the material ZDW,

#210165 - $15.00 USD Received 14 Apr 2014; revised 4 Jun 2014; accepted 13 Jun 2014; published 27 Jun 2014

but also of the material across the whole MIR region, for ultra-broadband MIR-SC sources based on chalcogenide SIF.

The material dispersion *D* was calculated from the standard formula [21]:

$$D = -\frac{\lambda}{c}\left(\frac{d^2 n}{d\lambda^2}\right) \tag{7}$$

where *n* is the refractive index at wavelength λ and *c* is the light velocity *in vacuo*. For AsSe and GeAsSe, the material dispersion obtained from Eq. (7), using the second derivative of the refractive index given by Eq. (5), is shown in Fig. 5. From Fig. 5, the material ZDW for As-Se, and Ge-As-Se, occurs at 7.4 μm and 7.0 μm, respectively. This may be compared with 7.2 for AsSe AMTIR-2 glass [10] as reported by Ung and Skorobogaty [24] who assumed that this was $As_{40}Se_{60}$ but from the published T_g [10] this seems not to be the correct stoichiometry (see section 4.4).

Importantly, from Fig. 5, it may also be seen that the material dispersion remains weak out to 20 μm wavelength.

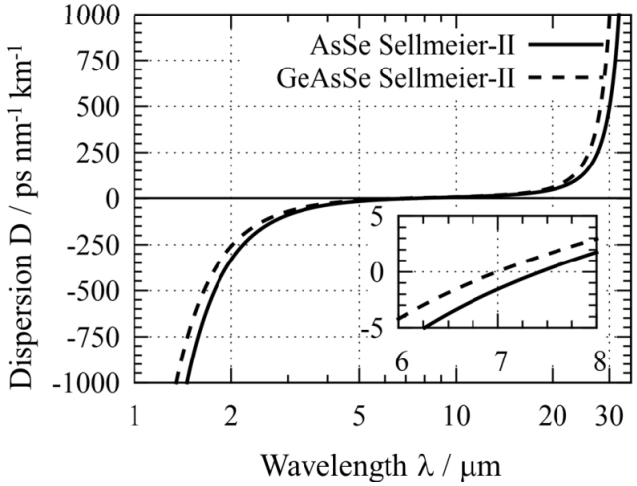

Fig. 5. Material dispersion D calculated from Eq. (7) and the fitted Sellmeier II (1,1) models of As-Se and Ge-As-Se. Inset: material dispersion close to the material ZDW.

5. Conclusions

Bulk glass samples AsSe and GeAsSe were prepared and analyzed for their refractive index dispersion by means of ellipsometry over the wavelength range: 0.4 – 33 μm. A Sellmeier two-term model, with one resonant VIS absorption and one resonant FIR absorption, was determined as sufficient for fitting the refractive index dispersion across the transparent window of each glass. We suggest that this is an analytical approach with potential for anticipating refractive index dispersion when the short and long wavelength resonant, intrinsic absorption of the chalcogenide glass composition is known. For the AsSe glass, the resonant FIR absorption (41.395 μm) corresponded with the literature value (41.7 μm). For the AsSe and GeAsSe glasses, the literature optical bandgaps (701 nm and 645 nm) respectively) corresponded with the onset of extinction (~700 nm and ~650 nm, respectively) but not with the modeled resonant photon energies, which were at higher energies. Material dispersion characteristics of the glasses, useful for SCG modeling, have been calculated. The material ZDW of As-Se, and Ge-As-Se, occurs at 7.4 μm and 7.0 μm, respectively, and the dispersion remains low out to 20 μm wavelength, whereafter it increases rapidly at longer wavelengths. We have calculated the *NA*, from the refractive indices measured using ellipsometry, for SIF composed of the AsSe core and GeAsSe cladding glass-pair and shown that it is higher than

#210165 - $15.00 USD Received 14 Apr 2014; revised 4 Jun 2014; accepted 13 Jun 2014; published 27 Jun 2014

0.97 over the entire wavelength range measured (0.4-33 μm). Our results show that this glass pair, which exhibits sufficiently matched thermal properties for SIF fabrication, which was experimentally demonstrated here, is a promising candidate for high *NA* chalcogenide glass SIF for broadband MIR-SCG.

Acknowledgments

This research has been partially supported by the European Commission through the Framework Seven (FP7) project MINERVA (317803; www.minerva-project.eu).

#210165 - $15.00 USD Received 14 Apr 2014; revised 4 Jun 2014; accepted 13 Jun 2014; published 27 Jun 2014